Cholinergic calcium responses in cultured antennal lobe neurons of the migratory locust

Gregor A. Bergmann* & Gerd Bicker*

University of Veterinary Medicine Hannover, Institute of Physiology and Cell Biology,

Bischofsholer Damm 15/102, 30173 Hannover, Germany

*Corresponding author

Abstract

Locusts are advantageous organisms to elucidate mechanisms of olfactory coding at the systems level. Sensory input is provided by the olfactory receptor neurons of the antenna, which send their axons into the antennal lobe. So far, cellular properties of neurons isolated from the circuitry of the olfactory system, such as transmitter-induced calcium responses, have not been studied. Biochemical and immunocytochemical investigations have provided evidence for acetylcholine as classical transmitter of olfactory receptor neurons. Here, we characterize cell cultured projection and local interneurons of the antennal lobe by cytosolic calcium imaging to cholinergic stimulation. We bulk loaded the indicator dye Cal-520 AM in dissociated culture and recorded calcium transients after applying cholinergic agonists and antagonists. The majority of projection and local neurons respond with increases in calcium levels to activation of both nicotinic and muscarinic receptors. In local interneurons, we reveal interactions lasting over minutes between intracellular signaling pathways, mediated by muscarinic and nicotinic receptor stimulation. The present investigation is pioneer in showing that Cal-520 AM readily loads *Locusta migratoria* neurons, making it a valuable tool for future research in locust neurophysiology, neuropharmacology, and neurodevelopment.

Key words: Calcium imaging; Olfactory system; ACh; nAChR; mAChR

1   **Introduction**

2   Migratory locusts are of socio-economical importance as devastating agricultural pests, but they serve

3   also in basic research as preparations for insect physiology, genomics, functional analysis of neural

4   circuitry, and for understanding underlying mechanisms of development[1-8]. In the field of systems

5   neurobiology, locusts have been instrumental to elucidate circuit mechanisms of olfactory coding in

6   the insect brain[9]. The antennal lobe (AL) is the primary olfactory center in insects, resembling the

7   olfactory bulb in mammals. Sensory input is provided by the olfactory receptor neurons (ORN) of the

8   antenna, which send their axons into the AL[10]. In this primary olfactory center, they make synaptic

9   connections with local interneurons and projection neurons. Similar to the architecture of the

10 vertebrate olfactory bulb, the synaptic terminals of insect ORN interact with the dendrites of local

11 interneurons and olfactory projection neurons in spherical neuropil compartments, termed glomeruli.

12 Most investigated insects, like for example the genetic model Drosophila, employ a uniglomerular

13 wiring strategy, in which ORN expressing the same olfactory receptor genes converge within the same

14 glomerulus in the AL[11,12]. Locusts, with their roughly 1000[13] glomeruli in the AL, provide a clear

15 exception of this principle.

16 In this wiring strategy, each ORN axon branches in the AL, innervating multiple glomeruli, where they

17 interface with both projection neurons (PN) and local interneurons (LN)[9,10,13,14]. Local interneurons,

18 the most common of which being GABAergic and nitrergic[15], also contact multiple glomeruli at once

19 and play a modulatory role in this network[16,17]. The dendrites of each projection neuron, in turn,

20 sample input from several glomeruli. The axons of the 830 olfactory projection neurons convey the

21 output of the AL to the mushroom body and the lateral horn[10,13,16,18]. Since the olfactory system is very

22 amenable both to anatomical and electrophysiological analysis[13,14,16-18], extensive knowledge about

23 odor encoding in the AL and the mushroom body has accumulated over the last four decades. Again,

24 similar to the olfactory bulb, odor stimulation leads to oscillatory activity in the AL[17]. This synchronized

25 electrical activity is generated through the recruitment of GABAergic inhibitory local neurons and

26 reflected in the temporal dynamics of firing patterns of the projection neurons toward the mushroom

27 body[17].

28 Immunocytochemical investigations show that sensory neurons of the antenna express the

29 acetylcholine synthetizing enzyme choline acetyltransferase, the vesicular acetylcholine transporter

30 and a high affinity choline transporter[19-22]. Based on these investigations of several working groups,

31 the majority of antennal ORN are thought to use acetylcholine as classical transmitter. There are two

32 fundamentally different receptor types for acetylcholine, which are also present in insects. Ionotropic

33 nicotinic acetylcholine receptors (nAChR) mediate mainly fast synaptic neurotransmission while

34 metabotropic muscarinic acetylcholine receptors (mAChR) are thought to have modulatory roles via

1 intracellular signal cascades, such as stimulation of phospholipase C, adenylate cyclase inhibition, and

2 cation conductance changes[23-26].

3 Unlike in the model organism Drosophila, where neural activity in defined of classes of neurons has

4 been visualized using targeted expression of genetically encoded calcium indicators[27-29], we are aware

5 of only one calcium imaging study in the locust olfactory system. To estimate odor-evoked neuronal

6 firing rate from Ca^{2+} signals, the calcium indicator Oregon-Green BAPTA-1 was injected into single

7 projection neurons which were imaged using two-photon microscopy[30]. So far, cellular properties of

8 neurons isolated from the circuitry of the olfactory system, such as transmitter-induced Ca^{2+}

9 responses, have not been reported.

10 In this investigation, we aim to establish a procedure to characterize large numbers of olfactory system

11 neurons by calcium imaging in dissociated cell culture. However, based on our own experience with

12 cultured locust neurons of thoracic ganglia, there are difficulties in recording cytosolic signals with a

13 number of commonly applied fluorescent calcium sensors in the acetoxymethyl ester (AM) form, due

14 to rapid intracellular compartmentalization and dye extrusion. Here, we use the next generation

15 calcium indicator Cal-520 AM to load AL neurons of *Locusta migratoria* and record their response to

16 cholinergic stimulation. To distinguish between classes of local and projection neurons in culture, we

17 label GABAergic and nitrergic LN[15,16] and develop additional criteria from measuring soma size for

18 appropriate identification. We find Ca^{2+} responses to cholinergic agonists in neurons of both classes.

19 We also show crosstalk between intracellular signaling pathways mediated by nicotinic and muscarinic

20 receptors. This opens new avenues to analyse transmitter-related properties of olfactory network

21 components of a pest insect in a controlled environment. Moreover, it allows for a comparison of

22 published cellular properties of AL neurons in the genetic model Drosophila[29] to those of an insect

23 relying on a different neuroanatomical wiring, but with well-investigated electrophysiology of the

24 olfactory system[9].

25

1   **Results**

2   *Cell populations of the antennal lobe*

3   To characterize neuronal phenotypes of the AL in the species *Locusta migratoria*, we started with a

4   survey of its complete number of cells. We counted DAPI-labeled nuclei on frontal tissue sections,

5   which were double-labeled for anti-acetylated tubulin (Fig.1a) and GABA (Fig.1b). Evaluation of the

6   composite allowed for a comparison of nuclear size (Fig.1c) of the GABAergic LN (Fig.1d) with the

7   remaining nuclei belonging to cells of undetermined transmitter phenotype. The AL comprised an

8   overall mean of 1422 cells (neurons plus glia), including 83 GABAergic LN (Tab.1). These cell counts

9   revealed no significant differences between males and females (Tab.1; p = 0.0823, p = 0.5368; Mann-

10   Whitney test).

11   For physiological characterization, we chose to isolate and culture AL neurons in order to remove

12   network interactions. In primary cell culture, we recovered 16.9 % (± 7.1 s.d. n = 29) of cells for

13   immune- and cytochemical characterization of GABAergic and nitrergic phenotype[15], indicative of local

14   neurons. The majority of neurons, presumably PN, were unlabeled cells with small somata of about

15   15 μm in diameter (Fig.2 arrows). In line with a previous histological study[15], GABA-IR (Fig.2a, b, c

16   asterisks), NADPHd positive (Fig.2d, e, f asterisks), and double labelled cells LN were also present

17   (Fig.2g, h, i asterisks). A fifth class comprised large neurons with soma diameters of about 20 μm and

18   no determined transmitter phenotype, presumably belonging to LN (Fig.2k, l, m asterisks).

19   To obtain a purposeful distinction between PN and LN, we initially quantified nucleus size from the

20   paraffin sections and cell culture. To avoid any erroneous inclusion of other brain parts and perineural

21   glia, we took care to evaluate only round nuclei in the anterior half of the AL[31]. Nuclei of GABA-IR

22   neurons (Mean: 16.35 μm ± 0.11 s.e.m. n = 500) were significantly larger than nuclei of all sampled AL

23   cells (Mean: 12.17 μm ± 0.07 s.e.m. n = 1716; p < 0.0001, Kruskal-Wallis test; Fig.3). Nuclear diameters

24   of GABA-IR neurons showed a normal distribution, whereas those of all measured cells did not (Fig.3a

25   & b; p = 0.66 and p < 0.0001 respectively; D'Agostino & Pearson normality test). Nuclear diameters of

26   GABAergic LN appeared to be a normally distributed subgroup of all nuclei (Fig.3b i), since their mean

27   diameter coincided with the plateau found in the tail of the distribution of all nuclei. For better

28   illustration, we normalized relative frequencies of the GABAergic LN nuclear diameters to the total

29   number of measured cells (Fig.3b).

30   Assuming that all LN nuclei are of similar size, we analyzed whether nuclear diameters of GABA-IR cells

31   could be used to estimate the percentage of LN (GABA-IR and other) in the AL. First, we calculated the

32   normalized frequency of non LN nuclear diameter as the difference of the normalized frequencies of

33   all cells and GABAergic LN. This uncovered the range of overlap in both distributions (Fig.3b ii). Both

1 distributions overlap considerably at diameters between 10 μm and 12 μm. Intriguingly, the

2 normalized frequency of the presumptive non LN nuclear diameters was close to zero at the mean LN

3 nuclear diameter, which allowed us to calculate the percentage of LN in the AL. We counted all cells

4 with nuclear diameters that were larger than the mean nuclear diameter of GABAergic LN

5 (representing 50 % of all LN), doubled the outcome and divided by the total number of measurements.

6 According to this calculation, roughly 24 % of AL cells are LN.

7 Based on nuclear diameter, PN and LN were not sufficiently distinguishable in culture. Due to losses

8 of very large cells, nuclei of cultured LN (14.88 μm ± 0.17 s.e.m. n = 178) appeared to be significantly

9 smaller than LN nuclei in sections (Fig.3a; $p < 0.0001$, Kruskal-Wallis test). Despite a statistically

10 significant difference between nuclear diameters of all measured neurons and labeled LN (Fig.3a, p =

11 0.0001, Kruskal-Wallis test), the normalized frequency of non LN at mean LN nucleus diameter was not

12 close to zero (Fig.3c ii). However, when soma diameter was used for LN classification, the normalized

13 frequency of non LN at mean LN soma diameter was close to zero (Fig.3d ii). Another way to evaluate

14 the suitability of a given classifier is the comparison of the area under respective receiver-operating

15 characteristic (ROC) curves, in which a larger area indicates a better classifier. ROC analysis confirmed

16 that soma diameter (Fig.3d iii; A = 0.924 ± 0.008 s.e.) is a better classifier than nuclear diameter (Fig.3c

17 iii; A = 0.835 ± 0.017 s.e.) for estimation of the LN population. Therefore, soma diameters of labeled

18 LN were used for the estimation of LN number in culture. Soma diameters of labeled LN were normally

19 distributed, whereas diameters of all neurons were not (Fig.3a, d; p = 0.275 and $p < 0.0001$

20 respectively; D'Agostino & Pearson normality test). Diameters of all measured neurons (15.97 μm ±

21 0.10 s.e.m. n = 1275) were significantly different ($p < 0.0001$, Kruskal-Wallis test) to diameters of

22 labeled LN (23.87 μm ± 0.87 s.e.m. n = 198). ROC analysis showed a classifier specificity of 0.94 at

23 mean LN soma diameter. We calculated a percentage of 10.2 % LN in the cultures, indicating a

24 preferential loss of LN over PN in the cell culture procedure. Additionally, the ROC analysis allowed to

25 calculate a criterion for the distinction between PN and LN based on soma diameter. At a threshold

26 diameter of 19.61 μm, the sensitivity was equal to the specificity on the ROC curve. Cells with soma

27 diameters smaller or larger than this threshold were predicted as PN or LN respectively and, from now

28 on, will be termed accordingly.

29 *Calcium imaging of cultured antennal lobe neurons*

30 After unsuccessful attempts with other indicators (Suppl. Tab. S1), we reliably detected calcimycin-

31 induced Ca^{2+} transients in cultured locust neurons by applying the calcium sensor Cal-520 AM. We

32 selected regions on the dish that contained PN and LN using the previously established criterion.

33 Following the imaging sessions, it was possible to verify a potential GABAergic or nitrergic phenotype

34 of LN by immunofluorescence and cytochemistry.

1 Cultured cells responded with pronounced Ca^{2+} transients when stimulated with the unspecific

2 cholinergic agonist carbachol (Fig.4a). Occasionally, they showed also spontaneous transients of lower

3 magnitude (Fig.4a, Suppl. Fig. S2). Inhibition of cholinergic receptors with specific antagonists reduced

4 the amplitude of responses, yielding a variety of outcomes (Fig.4).

5 In some PN, inhibition of muscarinic receptors with atropine resulted in a stronger reduction compared

6 to nicotinic receptor inhibition with tubocurarine, but we also imaged PNs with converse responses

7 (Fig.4a i and ii). Antagonists appeared to have stronger effects on labeled LN of GABAergic/nitrergic

8 phenotype (Fig.4a iii and iv).

9 To account for the multitude of effects, we normalized Ca^{2+} amplitudes in the presence of inhibitors to

10 the respective previous response to carbachol (Fig.4b). Atropine reduced carbachol responses in PN

11 to 70.68 % (± 5.29 s.e.m. n = 172). We found twelve labeled LN showing GABA-IR, four of which were

12 double-labeled for NADPHd activity. When pooled, atropine reduced LN responses to a mean of

13 41.64 % (± 6.95 s.e.m. n = 21) which was significantly different to PN response reduction (p = 0.0048,

14 Mann-Whitney test). Tubocurarine reduced PN amplitudes to 75.25 % (± 3.39 s.e.m. n = 172), and the

15 amplitudes of LN to 57.74 % (± 9.94 s.e.m. n = 21) of the previous response. We found no significant

16 differences in response reduction by tubocurarine between PN and LN (p = 0.0968, Mann-Whitney

17 test). These findings suggest that muscarinic and nicotinic acetylcholine receptor activation causes

18 Ca^{2+} transients in AL neurons.

19 Next, we examined whether LN and PN show different responses to stimulation with nicotinic and

20 muscarinic agonists (Fig.5, Suppl. Video S3). In range finding experiments, we determined that 1 µM

21 nicotine and 10 µM pilocarpine elicit Ca^{2+} transients of similar magnitude in the majority of PNs

22 (Fig.5a i). However, depending on the agonist and the individual neuron, responses were not entirely

23 consistent in amplitude. Alternating nicotine and pilocarpine stimulations revealed three basic

24 response types in PN with equal responses to both agonists, stronger responses to nicotine, and

25 stronger responses to pilocarpine (Fig.5a i-iii). To illustrate whether these response types follow a

26 certain distribution, we calculated the difference between the respective nicotine- and pilocarpine-

27 elicited amplitudes (ΔN – ΔP), and plotted their relative frequency in a histogram (Fig.5b). Averaged

28 over a large sample of 253 cultured neurons, the used concentrations elicited Ca^{2+} responses of similar

29 peak amplitude in roughly one third of PN (Fig.5b-d). LN showed a different behavior towards the

30 same experimental protocol.

31 Labeled LN frequently showed larger Ca^{2+} transients during muscarinic than nicotinic stimulation

32 (Fig.5a iv-vi). However, nicotine and pilocarpine responses were not consistent in amplitude, similar to

33 responses in PN. On average, nicotinic responses of LN subtypes were smaller in amplitude than

6

1   nicotinic responses of PN (Fig.5c). Pooling of these LN subtypes resulted in a mean nicotinic amplitude

2   of 20.51 %ΔF/F ($\pm$ 2.69 s.e.m. n = 30), which was significantly different to the respective response

3   amplitude of PN (Mean: 40.41 %ΔF/F $\pm$ 1.45 s.e.m. n = 253; p < 0.0001, Mann-Whitney test).

4   Pilocarpine responses of NADPHd positive LN were on average similar in amplitude to PN (Fig.5d). In

5   contrast, pilocarpine responses of exclusively GABAergic LN (56.7 %ΔF/F $\pm$ 11.70 s.e.m. n = 6) were

6   larger on average than PN amplitudes, whereas amplitudes of ND local neurons were lower (17.36

7   %ΔF/F $\pm$ 3.94 s.e.m. n = 16). This difference resulted in a mean response amplitude of 29.38 %ΔF/F

8   ($\pm$ 30.30 s.e.m. n = 2) when LN were pooled, which was not significantly different to PN amplitude (p =

9   0.3825, Mann-Whitney test).

10   To quantify the relationship between nicotinic and muscarinic responses in individual neurons, we

11   evaluated the difference of corresponding response amplitudes (ΔN - ΔP) (Fig.5e). LN (Mean: -9.77

12   %ΔF/F $\pm$ 4.17 s.e.m. n = 30) were significantly different (p < 0.0001; Mann-Whitney test) from PN

13   (Mean: 6.84 %ΔF/F $\pm$ 1.13 s.e.m. n = 253). This indicated that LN show stronger responses to

14   pilocarpine than to nicotine. Furthermore, exclusively GABAergic neurons (Mean: -36.33 %ΔF/F

15   $\pm$ 14.42 s.e.m. n = 6) seem to form a subset of local neurons that are characterized by larger Ca^{2+}

16   transients in response to pilocarpine.

17   Cholinergic neurotransmission can be modulated by crosstalk of intracellular signaling pathways

18   triggered by muscarinic and nicotinic receptor activation[32]. To detect potential interactions, we

19   utilized a shortened protocol with stimulations every 2 min for 15 s. The protocol consisted of two

20   1 µM nicotine pulses, one pulse of a co-applied nicotine/pilocarpine mixture (1 µM and 10 µM

21   respectively), another test pulse of nicotine, and a pulse of 10 µM pilocarpine. As a control, we

22   replaced the nicotine/pilocarpine pulse with a nicotine pulse in half of the experiments to determine

23   whether nicotinic stimulations yielded consistent responses. Projection neurons showed similar

24   transients during each nicotinic stimulation, both in co-application as well as in the control (Fig.6a i-iii,

25   b). On average, we found no significant differences between amplitudes of the control and the

26   respective amplitudes of the co-application protocol (Fig.6b; lowest p = 0.6986 N2 vs. N2; Kruskal-

27   Wallis test). In the example of Fig.6a i, co-stimulation elicited in the PN a larger transient than nicotine

28   alone, whereas pilocarpine alone induced a transient of similar magnitude. This was not the case for

29   all PN (Fig.6a ii-iii). To check whether such increased responses can be explained by a simple addition

30   of pilocarpine and nicotine-induced Ca^{2+} transients during co-application, we calculated the sum of the

31   nicotinic response (N2) prior to co-application and the respective muscarinic response (P) for each

32   neuron. We found no significant alterations in nicotinic responsiveness after co-stimulation in PNs (p

33   > 0.9999; Friedman test). Friedman's test for paired data revealed a significant difference between

34   the sum of nicotine and pilocarpine responses and the respective co-application (p < 0.0001).

1   Local neurons, however, responded notably different than PN. Labeled LN exhibited rather varied

2   responses. Whereas some showed enhanced nicotinic responses after co-application compared to

3   prior nicotinic responses (Fig.6a iv-vi), others showed no or weak responses to nicotine throughout the

4   experiment (Fig.6a vii-ix). We found enhanced nicotine responses after co-application in all three

5   labeled LN subtypes. These effects were also noticeable in larger mean response amplitude of the 31

6   pooled LN (Fig.6c). A significant difference (p = 0.0053; Kruskal-Wallis test) was only apparent between

7   the third nicotine stimulation in the control (N3) and the nicotine/pilocarpine stimulation in the co-

8   application (NP). The experimentally determined signal amplitude of co-application corresponded

9   nicely to the predicted calculated sum, as no significant difference between co-application and the

10 sum of nicotine and pilocarpine responses was found (Fig.6c; p = 0.1802; Friedman test). This indicated

11 that for LN, the response amplitude during co-stimulation is indeed the result of nicotinic and

12 muscarinic Ca^{2+} transient addition.

13 When we examined whether a co-stimulation of nicotinic and muscarinic receptors has notable effects

14 on following nicotinic stimulations for the pooled LN (Fig.6c), we measured a slight increase in mean

15 amplitude without statistical significance (p > 0.9999; Friedman test). This is likely accounted for by

16 heterogeneity in response levels and in contrast to findings in individual traces. To provide a more

17 detailed analysis of the enhanced response effect in LN after co-stimulation, and to compare it to

18 responses in PN, we calculated the difference of nicotinic amplitudes after and prior to co-application

19 (ΔN4 – ΔN2) in order to normalize for baseline responsiveness to either agonist (Fig.6d). This resulted

20 in tailed distributions of amplitude differences, reflecting response variability in individual PN and LN.

21 Most PN showed no or little change in amplitude (Mean: -1.56 %ΔF/F ± 1.17 s.e.m. n = 177). The

22 distribution of PN amplitude differences was tailed in both directions (Fig.6d). In contrast to PN, the

23 distribution of LN had a larger tail towards stronger nicotine responses after co-application (Mean:

24 19.02 %ΔF/F (± 6.58 s.e.m. n = 31). Amplitude differences of LN and PN were significantly different to

25 each other (p = 0.0073; Mann-Whitney test), revealing an enhanced responsiveness of LN to nicotinic

26 stimulation after co-application of a muscarinic agonist.

8

Discussion

In this investigation, we characterized AL neurons of *Locusta migratoria* neurons by calcium imaging in cell culture, focusing on the classical transmitter of the ORN, acetylcholine (ACh). We were motivated by other investigations that used calcium indicators in the AM form for recording ACh-induced cell responses in primary cultured insect neurons[33,34], and succeeded to obtain Ca^{2+} transients in the locust by loading the indicator Cal-520 AM (Fig.4; Suppl. Tab. S1). We showed that both PN and LN respond to nicotinic stimulation (Figs.4; 5). The majority of both types of neurons were also responsive to muscarinic stimulation, with local neurons as the more sensitive cellular phenotype (Fig.5). Simultaneous nicotinic and muscarinic stimulation of subsets of local neurons caused an enhanced Ca^{2+} response to a subsequent nicotine stimulus, indicating an intracellular interaction triggered by the activation of the two classes of cholinergic receptor types (Fig.6).

A prominent subset of the LN in the locust AL use GABA as classical neurotransmitter[9,15,16,35]. We utilized this information to distinguish between PN and LN in cell culture (Fig.3), without preceding labeling. Using ROC curves, we could approach the binary classification problem in culture by analyzing the prediction of the transmitter phenotype GABA from the soma diameter (Fig.3 iii). We settled for a criterion on the ROC curve, where the sensitivity is equal to the specificity, considering somata larger than a diameter of approximately 20 µm as LN and the PN as smaller. This procedural method, although afflicted with a small risk of inaccuracy, made it unnecessary to label neurons with tracers in the experimental animals prior to dissociation. Nonetheless, to confirm the GABAergic phenotype, all calcium imaging sessions were followed by labeling for GABA-IR.

Based on the simple assumption of a similar nuclear size distribution of GABA-positive LN and other unlabeled LN, we could also estimate the total number of LN from size measurements in tissue sections through the AL. These calculations excluded the glial cells, which make up 30% of locust brain cells[31]. Using the size distribution of DAPI-labeled nuclei of GABAergic neurons as proxy for all LN (Fig.3 a,b) we estimate that 24 % of the AL neurons are LN. This corresponds nicely to the 26% LNs which were reported for Schistocerca[9]. While the AL of Schistocerca seems to contain around 1130 neurons in total[9,16], we estimated about 1000 neurons in the AL of *Locusta migratoria*. The number and the ratio between LN and relaying PN is considered to be an important factor in the oscillatory transient synchronization of AL output during odor encoding in the intact animal[9]. Pharmacological blocking of the inhibitory synapse between the GABAergic LN to the PN abolishes spike synchronization without affecting the response pattern of each individual neuron[35].

For evaluation of responses to the cholinergic stimulation in cell culture, we chose the peak amplitude of the Ca^{2+} transients. In the diagrams we present separately the data for LN, that were immuno- and cytochemically (GABA, NADPH, double-labeled) characterized and the LN with not determined transmitter phenotype (ND). Due to a smaller sample size of neurons with confirmed neurotransmitter

9

1   phenotype, we chose to perform statistical tests only between all PN and LN, as defined by the ROC

2   method (Figs.4-6).

3   Similar to vertebrates, there are two fundamentally different receptor types for ACh in insects.

4   Ionotropic nicotinic AChR for fast synaptic neurotransmission and metabotropic muscarinic AChR with

5   modulatory functions via intracellular signal cascades[23-26]. In Locusta, five cDNA clones that encode

6   nAChR subunits have been identified[36]. As for all insect nAChR subunits, functional expression in

7   heterologous systems is not easy to achieve, but has been successful for an alpha-like subunit of

8   Schistocerca in Xenopus oocytes[37,38] and a novel beta subunit[39]. Modulation of ACh release from

9   synaptosome preparations provided biochemical evidence for muscarinic receptors in the CNS of

10   locusts[40,41]. The gain of the monosynaptic connection between the cholinergic locust wing stretch

11   receptor and an identified wing depressor motoneuron is modulated by muscarinic autoreceptors on

12   the presynaptic terminals of the stretch receptor itself and/or on muscarinic receptors of GABAergic

13   interneurons[42,43]. In intact Drosophila, muscarinic stimulation and blocking of mAChR diminish or

14   enhance Ca^{2+} transients of PN respectively during odor presentation[29]. In the same study, mAChR have

15   been demonstrated to increase LN excitability as a means to counteract short-term depression at the

16   ORN to LN synapse. Here we show that, compared to PN, especially GABAergic LN generate

17   considerably stronger Ca^{2+} transients in response to muscarinic stimulation, whereas their respective

18   nicotinic response appears to be lower than that of PN. However, unlike in Drosophila where PN do

19   not express mAChR[29], muscarinic stimulation elicited clear-cut Ca^{2+} transients in most locust PN (Fig.5).

20   Even though both the spiking PN and non-spiking LN receive cholinergic input from ORN axon terminals

21   in the glomeruli, both neuron types may react differently given their role in the olfactory circuit. This

22   was confirmed by comparing Ca^{2+} transients of LN and PN in response to nicotinic and muscarinic

23   agonists and pharmacological inhibition of their corresponding receptor types.

24   Surprisingly, co-stimulation enhanced subsequent nicotinic responses in some LN that showed no or

25   rather small Ca^{2+} signals to nicotine prior to co-stimulation (Fig6a iv, v). The mechanistic underpinnings

26   of these cellular phenomena and whether they are also involved in an increase in electrical excitability

27   remain to elucidated. After stimulation with nicotine, the intracellular Ca^{2+} concentration can increase

28   via influx through voltage-gated Ca^{2+} channels, through opening nAChR, and potentially by calcium-

29   induced Ca^{2+} release from intracellular stores. Combined voltage-clamping and calcium imaging of

30   dissociated somata from Locusta thoracic ganglia show that the influx through nAChR contributes to

31   about 25 % of the Ca^{2+} signal after carbachol stimulation[44]. Calcium ion fluxes do not only change

32   rapidly the membrane potential, but can also regulate signal transduction pathways on a longer

33   timescale. Intracellular Ca^{2+} accumulation may thus cause lasting plastic changes in the cell biology of

34   neurons. For example, Campusano et al.[45] decribed a form of neuronal plasticity for cultured

35   Drosophila Kenyon cells, in which a brief conditioning pulse of nicotine causes a decrease in

1   responsivenes to a second nicotine application 4 h later. In contrast, we detected an enhancement in

2   nicotine-induced Ca^{2+} responses after co-stimulation with nicotine and pilocarpine that seems to be a

3   distinctive feature of a group of local neurons including some of the GABAergic LN (Fig.6d). The cellular

4   memory of this form of plasticity lasts for at least 2 minutes. Potentially, neuromodulation by

5   muscarinic receptors may upregulate the fast synaptic transmission via nicotinic receptors in the intact

6   AL[29].

7   A subset of LN releases NO in a calcium-dependent manner that stimulates the formation of cGMP in

8   the same or other LN[15,46,47]. In our calcium imaging study, we also found examples of these LN which

9   were responsive both to stimulation with nicotine and pilocarpine (Fig.5a v vi, c-e).   Further

10   investigations must show how increases in cGMP levels may in turn regulate intracellular Ca^{2+} levels

11   and neuronal excitability.

12   We have also found spontaneous Ca^{2+} transients mainly in PNs that occured prior to carbachol

13   stimulation, but also later at regular intervals between stimulation events. Since the shown traces in

14   the Suppl. Fig. S2 were not from neurons linked by neurites, these transient do not reflect network

15   activity. Rather they reflect cell intrinsic oscillations of similar frequency and amplitude (Suppl. Fig S2

16   a) and also irregular fluctions (b) of Ca^{2+} concentrations. In Drosophila cell cultures, spontaneous Ca^{2+}

17   transients are also generated by Kenyon cells and about 60% of all central brain neurons[48]. Whether

18   neuronal Ca^{2+} transients are present in the developing and adult locust nervous system remains a

19   challenging question for future investigations.

20   So far, calcium imaging of locust neurons required intracellular injection of calcium indicators[30,44,49],

21   making simultaneous calcium imaging of large cell populations difficult. However, Isaacson and

22   Hedwig described an innovative technique, in which calcium indicators were introduced via

23   iontophoresis through the nerve sheath to multiple cells[50]. This method appears technically feasible

24   for easily accessible nerves, but may be rather difficult to apply for loading neurons of tracts running

25   in the depth of the brain, such as the antennal lobe tract. The present investigation is pioneer in

26   showing that Cal-520 AM readily loads *Locusta migratoria* neurons, making it a valuable tool for future

27   research in locust physiology. The genome of the migratory locust had been sequenced a few years

28   ago[1] which, alongside advancements in genome editing like CRISPR-Cas9, rekindled the interest in

29   research regarding the locust olfactory system[51]. Moreover, recent investigations introduced locusts

30   as helpful organisms for research on axonal regeneration in the olfactory system[52] and as predictive

31   test system for developmental neurotoxicity in humans[53,54]. Both lines of research will require

32   information how locust neurons exposed to axonal injury or developmental-toxicants respond to

33   these challenges in terms of Ca^{2+} concentration changes. Taken together, the possibility of calcium

34   imaging of selected neuronal populations in a defined environment has the potential to unravel new

35   insight into the cellular properties of the olfactory system of a devastating pest insect, which is also a

1   fruitful preparation for basic neurobiology.

2

3

4   **Methods**

5   Locusts (*Locusta migratoria*) from our crowded culture were used for cell culture of antennal lobe

6   neurons and paraffin sectioning. Locust brains were dissected in sterile Leibovitz's L15 containing 1 %

7   penicillin/streptomycine (Invitrogen). All chemicals were purchased from Sigma, unless noted

8   otherwise.

9   *Primary antennal lobe neuron culture*

10   For primary antennal lobe culture, the cell culture protocol of Kirchhof and Bicker[55] was modified. A

11   minimum of ten brains of an equal number of male and female fifth instar larvae were dissected at

12   room temperature. For optimal culturing of AL neurons, we used brain tissue from animals 1 - 3 days

13   after molting. Brains were desheathed, partially lifting the AL away from the protocerebrum, allowing

14   for easy removal with sharp forceps (see Suppl. Fig. S4).

15   In paraffin sections, we found no neuronal connections between the dorsal side of the antennal lobe

16   and the protocerebrum (Fig.1 d, segmented line). Therefore, it is very unlikely that the removal of the

17   antennal lobes removes a significant number of non antennal lobe neurons.

18   AL were incubated for 45 minutes in in sterile collagenase/dispase (1mg/ml in PBS, Roche), which was

19   subsequently removed by five 5 minute washing steps with L15 medium. Tissue was mechanically

20   dissociated by gentle up and down pipetting using a 200 µl siliconized pipette tip (VWR cat No. 53503-

21   794). The resulting suspension was seeded in small 20 - 50 µl droplets on ibiTreat µ-Dishes (Ibidi cat

22   No. 81156). Cells were allowed to adhere for 40 min, cultured at 30 °C in 3 ml L15 medium, and washed

23   thoroughly every two days. To select for neurons, cells were kept in culture for at least seven days,

24   since glia is not as viable in culture and dies within one week[31,55].

25   *Calcium imaging*

26   After unsuccessful attempts with several other calcium indicators (see Suppl. Tab. S1), we detected

27   calcimycin elicited Ca^{2+} transients in cultured locust neurons by applying the calcium sensor Cal-520

28   AM. Prior to loading, cultured neurons were washed for 10 min with L15 medium (supplemented with

29   10 mM HEPES, adjusted to pH 7.3; Roth). Optimal loading of AL neurons was achieved with 8 µM Cal-

30   520 AM calcium indicator (stock solution 8 mM in DMSO, Abcam cat No. ab171868) in L15/HEPES and

31   an incubation time of 90 minutes at 30 °C. For laminar superfusion of chemicals, a Warner RC-37W

32   perfusion insert was fitted into the culture dish. This setup was mounted on a Zeiss Axiovert 200

33   inverse epifluorescence microscope and connected to an open peristaltic perfusion system, delivering

1   a constant stream of L15/HEPES at 4 ml/min.

2   The indicator fluorescence was detected at excitation with 475 nm light (Colibri 7; filter set 44; ZEISS).

3   To reduce photobleaching and phototoxicity, images were taken every two seconds at 2 % light source

4   intensity, 4x4 binning (Axiocam 503 mono; Zeiss), 2x signal amplification, and an exposure time of

5   500 ms. For image acquisition ZEN 2.6 Imaging software (ZEISS) was used.

6   All cholinergic agonists and antagonists were dissolved and diluted in L15/HEPES. Carbachol, nicotine,

7   pilocarpine, and the calcium ionophore calcimycin (5 µM, stock solution 5 mM in DMSO) were applied

8   via a 3-way valve which was installed between the medium reservoir and the peristaltic perfusion

9   pump (mdx-biotechnik cat No. TL/150). Atropine and tubocurarine were applied by switching from

10   the main L15/HEPES reservoir to a separate reservoir containing the antagonist solutions.   For

11   antagonist experiments (Fig.4), we superfused cultured antennal lobe neurons every 10 min for 1 min

12   with 10 µM of the nonspecific cholinergic agonist carbachol. Using carbachol instead of acetylcholine

13   avoided rapid breakdown by catalytic activity of acetylcholinesterase which is expressed on the soma

14   surface of the majority of cultured locust neurons[56]. To probe for nicotinic or muscarinic components

15   in the Ca^{2+} transients, every other carbarchol stimulus was applied in the presence of equimolar

16   concentrations of an antagonist.   We chose the muscarinic antagonist atropine and the nicotinic

17   antagonist tubocurarine, which were pre-incubated for 5 min prior to carbachol stimulation.   For

18   agonist experiments (Fig.5), we stimulated cultured neurons with alternating 1 min nicotine and

19   pilocarpine superfusions separated by 9 min washout periods. For the experiments shown in Fig.6, a

20   shortened protocol with 15 second stimulations with the appropriate agonists and 105 seconds of

21   washout was used. In co-application experiments, following agonists were applied in consecutive

22   order: 1 µM nicotine; 1 µM nicotine; 1 µM nicotine + 10 µM pilocarpine; 1 µM nicotine; 10 µM

23   pilocarpine. For the respective control, the nicotine pilocarpine mix was replaced by 1 µM nicotine.

24   *NADPH-diaphorase staining and GABA-immunocytochemistry of cell culture*

25   For identification of the GABAergic and nitrergic phenotype of LN, cells were processed for GABA-IR

26   and NADPH-diaphorase (NADPHd) activity[46]. After image acquisition, cells were fixed in cold GPFA (4 %

27   paraformaldehyde dissolved in PBS with 0.1 % glutaraldehyde) on ice for 20 min, and rinsed with PBS

28   (10 mM sodium phosphate, 150 mM NaCl, pH 7.4; Roth). Subsequently, fixed cells were washed two

29   times in PBS-T (0.1 % Triton X-100; Roth) and once in 50 mM Tris HCl (pH 7.8, 0.1 % Triton; Roth).

30   NADPHd activity was visualized by incubating with 50 mM Tris HCl containing 0.24 mM β-NADPH and

31   0.24 mM nitroblue tetrazolium for 20 min at room temperature, until stained LN acquired a dark violet

32   color. Afterwards, cells were permeabilized with 0.3 % saponine in PBS-T for 20 min, washed and

33   blocked with 5 % normal goat serum (Linaris) in PBS-T. The primary rabbit antibody against GABA

34   (1:5000 in blocking solution; Sigma cat No. A2052) was incubated overnight at 4 °C. After three

1   washing steps in PBS-T, cells were incubated with secondary biotinylated goat anti-rabbit (1:333 in

2   blocking solution; Vector cat No. BA-1000) for at least 4 h at room temperature, followed by three

3   more washing steps. GABA-IR was visualized by incubation with streptavidin conjugated Cy3 (1:333 in

4   PBS-T) for at least 4 h at room temperature. Nuclei were labeled with 0.05 µg/ml 4',6-Diamidino-2-

5   Phenylindole (DAPI) simultaneously with the GABA-IR detection. For estimation of cell populations

6   within the antennal lobe culture, we measured soma and nuclear diameters of cells within the field of

7   view, as well as additional labeled LN outside the imaging frame. Since neurons can assume ellipsoid

8   or spindle like shapes, we measured the minimal and the maximal diameter of somata and nuclei for

9   each cell and used the mean.

10 *Paraffin sections and GABA-immunofluorescence*

11 Paraffin sectioning of locust brains (Tab.1) was performed as described by Stern et. al.[57]. Briefly, brains

12 were dissected in L15 medium, fixed in GPFA for 30 min at room temperature, rinsed in PBS,

13 dehydrated, embedded in paraffin (Roth), sectioned at 14 µm, and mounted on chromealum/gelatin

14 coated slides. Sections were rehydrated and washed in PBS. Immunolabeling was performed as in

15 culture, including an additional labeling against acetylated-α-tubuline (monoclonal, 1:1000 in blocking

16 solution; Sigma cat No. T6793), which was detected with Alexa488 conjugated goat anti-mouse (1:250

17 in blocking solution; Invitrogen cat No. A11001). A GABA-IR detection system (secondary antibody and

18 streptavidin-Cy3) was used at 1:250 respectively, and DAPI was used at 0.1 µg/ml. Slices were washed,

19 and cleared in glycerol. Nuclei within the antennal lobe were counted and evaluated according to the

20 Abercrombie correction[58]. For determination of nuclear diameters, 1716 randomly selected cells were

21 measured. Since nuclei of GABA-IR cells in the antennal lobe were generally larger in diameter, GABA-

22 IR cells were counted and cell number was corrected separately, using diameters of 500 GABA positive

23 cells. These measurements served to estimate the population of LN within the intact antennal lobe.

24 *Analysis of AL neuron types*

25 To analyze cell populations, we generated histograms of nuclear and soma diameters (Fig.3 b-d i).

26 Histograms shown in Fig.3 b-d ii were normalized to the nucleus/soma diameter distribution of all

27 measured cells, which include LN as well as PN. The diameter distribution of non LN was calculated by

28 subtracting the normalized frequencies of GABA-IR neurons from the normalized frequencies of all

29 measured cells (Fig.3 b-d ii). Since the normalized frequency of non LN at the mean LN diameter is

30 close to zero, LN percentage was calculated as follows. All cells with nucleus/soma diameters that

31 were larger than the mean LN nucleus/soma diameter, representing 50 % of the total LN population,

32 were counted, doubled and divided by the total number of cells. ROC curves were generated using

33 the Wilson/Brown method in GraphPad Prism 7, based on nucleus/soma diameters obtained from

34 sections and from cultured cells.

14

1   *Analysis of calcium imaging data*

2   Fluorescence of individual Cal-520 AM loaded cells was measured in Fiji[59] using manually fitted ROIs

3   for each cell. Background fluorescence at each given frame was subtracted from individual cellular

4   fluorescence. Baseline pre-treatment fluorescence (F) was measured 10 min prior to the first drug

5   application. The change of fluorescence relative to baseline (ΔF/F) was calculated and normalized to

6   the peak amplitude of the signal from stimulation with the calcium ionophore calcimycin (% ΔF/F). The

7   amplitudes of Ca^{2+} responses to pharmacological stimulation (e.g. ΔN for nicotinic stimulation) were

8   calculated as the difference of peak % ΔF/F and baseline fluorescence for each cell within a stimulation

9   period. Cells with changes in fluorescence above 110 % relative to calcimycin were considered as

10 damaged and thus excluded form data analysis. We did not apply this criterion for experiments of

11 Fig.6 to preserve increased transients beyond the calcimycin maximum. In this experiment, we

12 calculated a predicted value for co-application by simply adding amplitudes of the second nicotinic

13 stimulation (N2) to the respective pilocarpine amplitude in each cell (Fig.6 b)**.** This was necessary,

14 since the first nicotinic stimulation (N1) tended to elicit slightly larger Ca^{2+} transients in control as well

15 as in co-application experiments, and the nicotinic stimulation after co-application (N4) could be

16 affected by the previous stimulation of mAChRs.

17 *Statistical analysis*

18 Non-parametric tests were used for statistical analysis, since not all datasets showed normal

19 distribution. All tested comparisons were considered significant at alpha < 0.05. Kurskal-Wallis tests

20 for comparison of multiple datasets were performed with Dunn's correction. Two tailed Mann-

21 Whitney tests were used for comparing datasets with two groups (i.e. male vs. female or LN vs. PN).

22 Due to lower sample sizes, LN subtypes were not tested against PN. Friedman's test with Dunn's

23 correction was used for paired data. Error bars represent s.e.m. Calculation of ΔF/F, % ΔF/F, as well

24 as statistical analysis was performed in GraphPad Prism 7, Ca^{2+} response amplitudes were calculated

25 via Microsoft Excel, and R Studio version 1.3.1056 was used for data management.

26 *Data availability*

27 Data used in this study are available on reasonable request.

References

1   Wang, X. *et al.* The locust genome provides insight into swarm formation and long-distance flight. *Nat Commun* **5**, 2957, doi:10.1038/ncomms3957 (2014).

2   Zhang, L., Lecoq, M., Latchininsky, A. & Hunter, D. Locust and Grasshopper Management. *Annual Rev Entomol* **64**, 15-34 (2019).

3   Verlinden, H. *et al.* First draft genome assembly of the desert locust, Schistocerca gregaria. *F1000Research* **9**, 775, doi:10.12688/f1000research.25148.1 (2020).

4   Guo, X. *et al.* 4-Vinylanisole is an aggregation pheromone in locusts. *Nature* **584**, 584-588 (2020).

5   Burrows, M. *Neurobiology of an Insect Brain*. (Oxford University Press, 1996).

6   Roeder, T. Biochemistry and molecular biology of receptors for biogenic amines in locusts. *Microsc Res Tech* **56**, 237-247 (2002).

7   Goodman, C. S. & Bate, M. Neuronal development in the grasshopper. *Trends Neurosci* **4**, 163 - 169 (1981).

8   Truman, J., Ewer, J. & Ball, E. Dynamics of cyclic GMP levels in identified neurones during ecdysis behaviour in the locust Locusta migratoria. *J Exp Biol* **199**, 749-758 (1996).

9   Laurent, G. Dynamical representation of odors by oscillating and evolving neural assemblies. *Trends Neurosci* **19**, 489-496 (1996).

10   Hansson, B. S. & Stensmyr, M. C. Evolution of insect olfaction. *Neuron* **72**, 698-711 (2011).

11   Vosshall, L. B., Amrein, H., Morozov, P. S., Rzhetsky, A. & Axel, R. A spatial map of olfactory receptor expression in the Drosophila antenna. *Cell* **96**, 725-736 (1999).

12   Buck, L. & Axel, R. A novel multigene family may encode odorant receptors: a molecular basis for odor recognition. *Cell* **65**, 175-187 (1991).

13   Anton, S. & Hansson, B. S. Antennal lobe interneurons in the desert locust Schistocerca gregaria (Forskal): processing of aggregation pheromones in adult males and females. *J Comp Neurol* **370**, 85-96 (1996).

14   Ernst, K. D., Boeckh, J. & Boeckh, V. A neuroanatomical study on the organization of the central antennal pathways in insects. *Cell Tissue Res* **176**, 285-306 (1977).

15   Seidel, C. & Bicker, G. Colocalization of NADPH-diaphorase and GABA-immunoreactivity in the olfactory and visual system of the locust. *Brain Res* **769**, 273-280 (1997).

16   Leitch, B. & Laurent, G. GABAergic synapses in the antennal lobe and mushroom body of the locust olfactory system. *J Comp Neurol* **372**, 487-514 (1996).

17   Laurent, G. Olfactory network dynamics and the coding of multidimensional signals. *Nat Rev Neurosci* **3**, 884-895 (2002).

18   Laurent, G. & Naraghi, M. Odorant-induced oscillations in the mushroom bodies of the locust. *J Neurosci* **14**, 2993-3004 (1994).

19   Lutz, E. M. & Tyrer, N. M. Immunohistochemical localization of choline acetyltransferase in the central nervous system of the locust. *Brain Res* **407**, 173-179 (1987).

20   Knipper, M., Strotmann, J., Mädler, U., Kahle, C. & Breer, H. Monoclonal antibodies against the high affinity choline transport system. *Neurochem Int* **14**, 217-222 (1989).

21   Rind, F. C. & Leitinger, G. Immunocytochemical evidence that collision sensing neurons in the locust visual system contain acetylcholine. *J Comp Neurol* **423**, 389-401 (2000).

22   Ehrhardt, E. & Boyan, G. Evidence for the cholinergic markers ChAT and vAChT in sensory cells of the developing antennal nervous system of the desert locust Schistocerca gregaria. *Invert Neurosci* **20**, 19, doi:10.1007/s10158-020-00252-4 (2020).

23   Breer, H. & Sattelle, D. B. Molecular properties and functions of insect acetylcholine receptors. *J Insect Physiol* **33**, 771 - 790 (1987).

24   Gundelfinger, E. D. How complex is the nicotinic receptor system of insects? *Trends Neurosci* **15**, 206-211 (1992).

25   Caulfield, M. P. Muscarinic receptors--characterization, coupling and function. *Pharmacol Ther* **58**, 319-379 (1993).

26   Trimmer, B. A. Characterization of a muscarinic current that regulates excitability of an identified insect motoneuron. *J Neurophysiol* **72**, 1862-1873 (1994).

27   Fiala, A. *et al.* Genetically expressed cameleon in Drosophila melanogaster is used to visualize olfactory information in projection neurons. *Curr Biol* **12**, 1877-1884 (2002).

28   Wang, J. W., Wong, A. M., Flores, J., Vosshall, L. B. & Axel, R. Two-photon calcium imaging reveals an odor-evoked map of activity in the fly brain. *Cell* **112**, 271-282 (2003).

29   Rozenfeld, E., Lerner, H. & Parnas, M. Muscarinic Modulation of Antennal Lobe GABAergic Local Neurons Shapes Odor Coding and Behavior. *Cell Rep* **29**, 3253-3265.e4 (2019).

30   Moreaux, L. & Laurent, G. Estimating firing rates from calcium signals in locust projection neurons in vivo. *Front Neural Circuits* **1**, 2, doi:10.3389/neuro.04.002.2007 (2007).

31   Gocht, D., Wagner, S. & Heinrich, R. Recognition, presence, and survival of locust central nervous glia in situ and in vitro. *Microsc Res Tech* **72**, 385-397 (2009).

32   Trimmer, B. A. Current excitement from insect muscarinic receptors. *Trends Neurosci* **18**, 104-111 (1995).

33   Bicker, G. & Kreissl, S. Calcium imaging reveals nicotinic acetylcholine receptors on cultured mushroom body neurons. *J Neurophysiol* **71**, 808-810 (1994).

34   Cayre, M., Buckingham, S. D., Yagodin, S. & Sattelle, D. B. Cultured insect mushroom body neurons express functional receptors for acetylcholine, GABA, glutamate, octopamine, and dopamine. *J Neurophysiol* **81**, 1-14 (1999).

35   MacLeod, K. & Laurent, G. Distinct mechanisms for synchronization and temporal patterning of odor-encoding neural assemblies. *Science* **274**, 976-979 (1996).

36   Hermsen, B. *et al.* Neuronal nicotinic receptors in the locust Locusta migratoria. Cloning and expression. *J Biol Chem* **273**, 18394-18404 (1998).

37   Marshall, J. *et al.* Sequence and functional expression of a single alpha subunit of an insect nicotinic acetylcholine receptor. *Embo j* **9**, 4391-4398 (1990).

38   Amar, M., Thomas, P., Wonnacott, S. & Lunt, G. G. A nicotinic acetylcholine receptor subunit from insect brain forms a non-desensitising homo-oligomeric nicotinic acetylcholine receptor when expressed in Xenopus oocytes. *Neurosci Lett* **199**, 107-110 (1995).

39   Jones, A. K. *et al.* Sgbeta1, a novel locust (Schistocerca gregaria) non-alpha nicotinic acetylcholine receptor-like subunit with homology to the Drosophila melanogaster Dbeta1 subunit. *Invert Neurosci* **5**, 147-155 (2005).

40   Breer, H. & Knipper, M. Characterization of acetylcholine release from insect synaptosomes. *Insect Biochemistry* **14**, 337 - 344 (1984).

41   Knipper, M. & Breer, H. Subtypes of muscarinic receptors in insect nervous system. *Comp Biochem Physiol C* **90**, 275 - 280 (1988).

42   Leitch, B. & Pitman, R. M. Modulation of transmitter release from the terminals of the locust wing stretch receptor neuron by muscarinic antagonists. *J Neurobiol* **28**, 455-464 (1995).

43   Judge, S. & Leitch, B. Modulation of transmitter release from the locust forewing stretch receptor neuron by GABAergic interneurons activated via muscarinic receptors. *J Neurobiol* **40**, 420-431 (1999).

44   Oertner, T. G., Single, S. & Borst, A. Separation of voltage- and ligand-gated calcium influx in locust neurons by optical imaging. *Neurosci Lett* **274**, 95-98 (1999).

45   Campusano, J. M., Su, H., Jiang, S. A., Sicaeros, B. & O'Dowd, D. K. nAChR-mediated calcium responses and plasticity in Drosophila Kenyon cells. *Dev Neurobiol* **67**, 1520-1532 (2007).

46   Müller, U. & Bicker, G. Calcium-activated release of nitric oxide and cellular distribution of nitric oxide-synthesizing neurons in the nervous system of the locust. *J Neurosci* **14**, 7521-7528 (1994).

47   Bicker, G., Schmachtenberg, O. & Vente, J. D. Geometric considerations of nitric oxide-cyclic GMP signalling in the glomerular neuropil of the locust antennal lobe. *Proc R Soc Lond B* **264**, 1177-1181 (1997).

48   Jiang, S. A., Campusano, J. M., Su, H. & O'Dowd, D. K. Drosophila mushroom body Kenyon cells generate spontaneous calcium transients mediated by PLTX-sensitive calcium channels. *J Neurophysiol* **94**, 491-500 (2005).

49   Bentley, D., Guthrie, P. B. & Kater, S. B. Calcium ion distribution in nascent pioneer axons and coupled preaxonogenesis neurons in situ. *J Neurosci* **11**, 1300-1308 (1991).

50   Isaacson, M. D. & Hedwig, B. Electrophoresis of polar fluorescent tracers through the nerve sheath labels neuronal populations for anatomical and functional imaging. *Scientific Reports* **7**, 40433, doi:10.1038/srep40433 (2017).

51   Li, Y. *et al.* CRISPR/Cas9 in locusts: Successful establishment of an olfactory deficiency line by targeting the mutagenesis of an odorant receptor co-receptor (Orco). *Insect Biochem Mol Biol* **79**, 27-35 (2016).

52   Bicker, G. & Stern, M. Structural and Functional Plasticity in the Regenerating Olfactory System of the Migratory Locust. *Front Physiol* **11**, 608661, doi:10.3389/fphys.2020.608661 (2020).

53   Bergmann, G. A. *et al.* An intact insect embryo for developmental neurotoxicity testing of directed axonal elongation. *ALTEX* **36**, 643-649 (2019).

54   Bode, K. *et al.* A locust embryo as predictive developmental neurotoxicity testing system for pioneer axon pathway formation. *Arch Toxicol* **94**, 4099-4113 (2020).

55   Kirchhof, B. & Bicker, G. Growth properties of larval and adult locust neurons in primary cell culture. *J Comp Neurol* **323**, 411-422 (1992).

56   Bicker, G., Naujock, M. & Haase, A. Cellular expression patterns of acetylcholinesterase activity during grasshopper development. *Cell Tissue Res* **317**, 207-220 (2004).

57   Stern, M. *et al.* Development of nitrergic neurons in the nervous system of the locust embryo. *J Comp Neurol* **518**, 1157-1175 (2010).

58   Abercrombie, M. Estimation of nuclear population from microtome sections. *Anat Rec* **94**, 239-247 (1946).

59   Schindelin, J. *et al.* Fiji: an open-source platform for biological-image analysis. *Nat Methods* **9**, 676-682 (2012).

Acknowledgements

Author-Contributions

GAB conceived, performed, analyzed the experiments and wrote the paper with the help of GB. GB conceived and supervised the research.

Additional Information

Competing interests

The authors declare no competing interests.

Corresponding authors

Gerd Bicker: gerd.bicker@tiho-hannover.de   ORCID 0000-0003-3158-067X

Gregor A. Bergmann: gregor.bergmann@tiho-hannover.de   ORCID 0000-0001-9191-3072

1 **Tables**

2 **List of abbreviations**

AL	Antennal lobe
ORN	Olfactory recetor neuron
PN	Projection neurons
LN	Local neurons
GABA-IR	GABA immunoreactivity
NADPHd	NADPH diaphorase
nAChR	Nicotinic acetylcholine receptor
mAChR	Muscarinic acetylcholine receptor
ROC	Reciever operating characteristic

3

4

5 **Table 1: Comparison of nuclear countings from antennal lobe of female and male migratory locusts.**
6 Nuclei of 11 antennal lobes (AL) from seven individuals were analyzed. Nuclear counting comprises PN,
7 LN, and glia. Mann-Whitney tests revealed, that nucleus counts of all cells and GABAergic cells was not
8 significantly different between male and female locusts ($p = 0.0823$; $p = 0.5368$ respectively).

	Female	Male	All
# Individuals	3	4	7
# AL imaged	5	6	11
Mean # Cells	1347 ± 104.1 s.e.m.	1484 ± 105.1 s.e.m.	1422 ± 73.81 s.e.m.
Mean # GABA	86.8 ± 10.05 s.e.m.	79.9 ± 18.56 s.e.m.	83.0 ± 5.93 s.e.m.

9

1   **Figures**

2
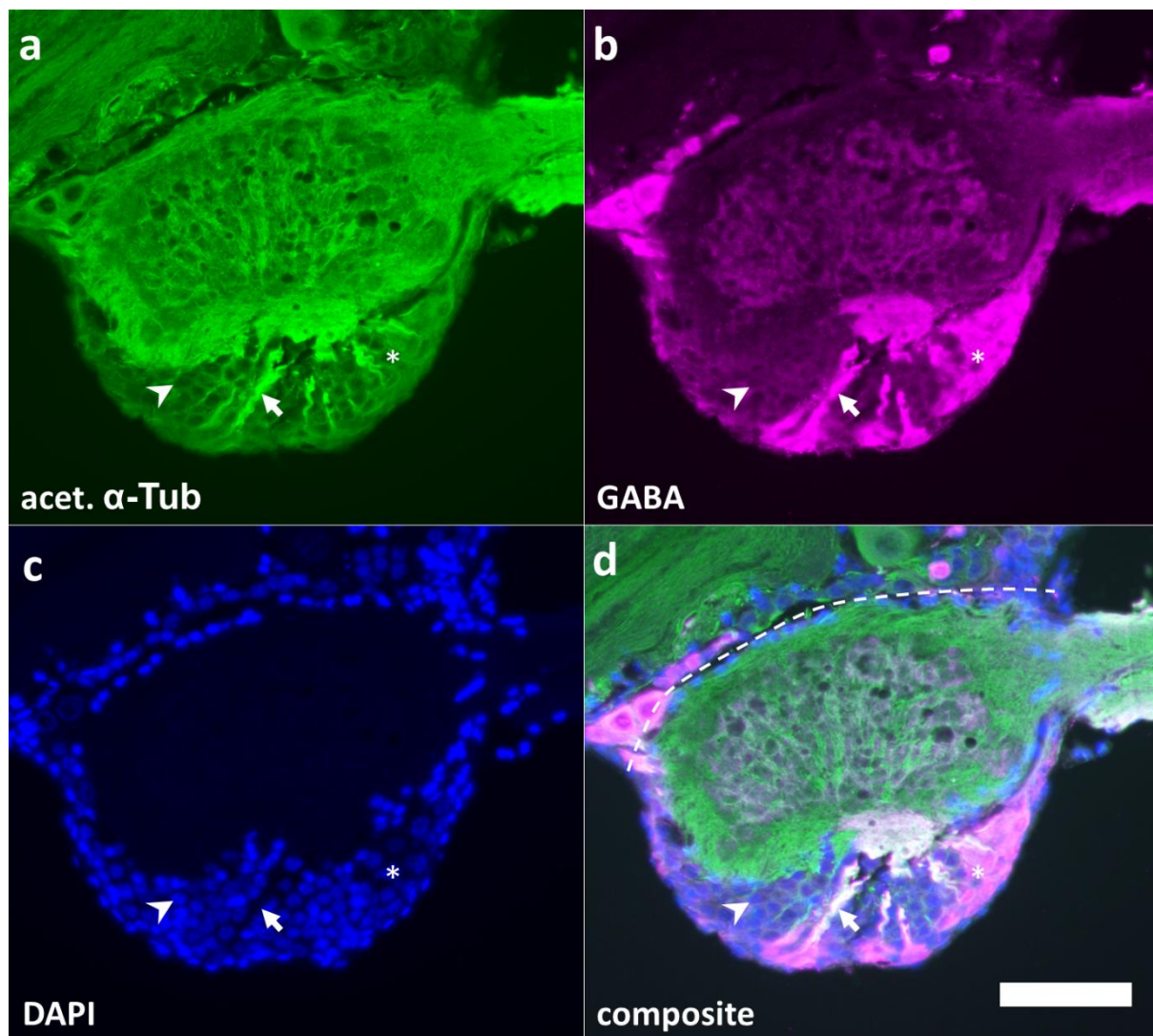
3   **Figure 1: Frontal sections through the antennal lobe of *Locusta migratoria*.** Sections were labeled
4   using anti-acetylated α-tubuline (**a**) and anti-GABA (**b**) antisera, and the nuclear marker DAPI (**c**). GABA-
5   IR local neurons (asterisk) were found in the frontal cell group of the antennal lobe. Somata of GABA-
6   IR local neurons were typically larger compared to other cells (**c**). Most PN are also found in the frontal
7   cell group, but had significantly smaller nuclei (arrowhead). In **d**, white color indicates colocalisation of
8   GABA and acetylated α-tubuline. GABAergic LN and PN arborize into glomeruli (arrow). No arbors or
9   connecting neurites were found on the dorsal side of the antennal lobe (segmented line). Scalebar =
10   100 μm.

1
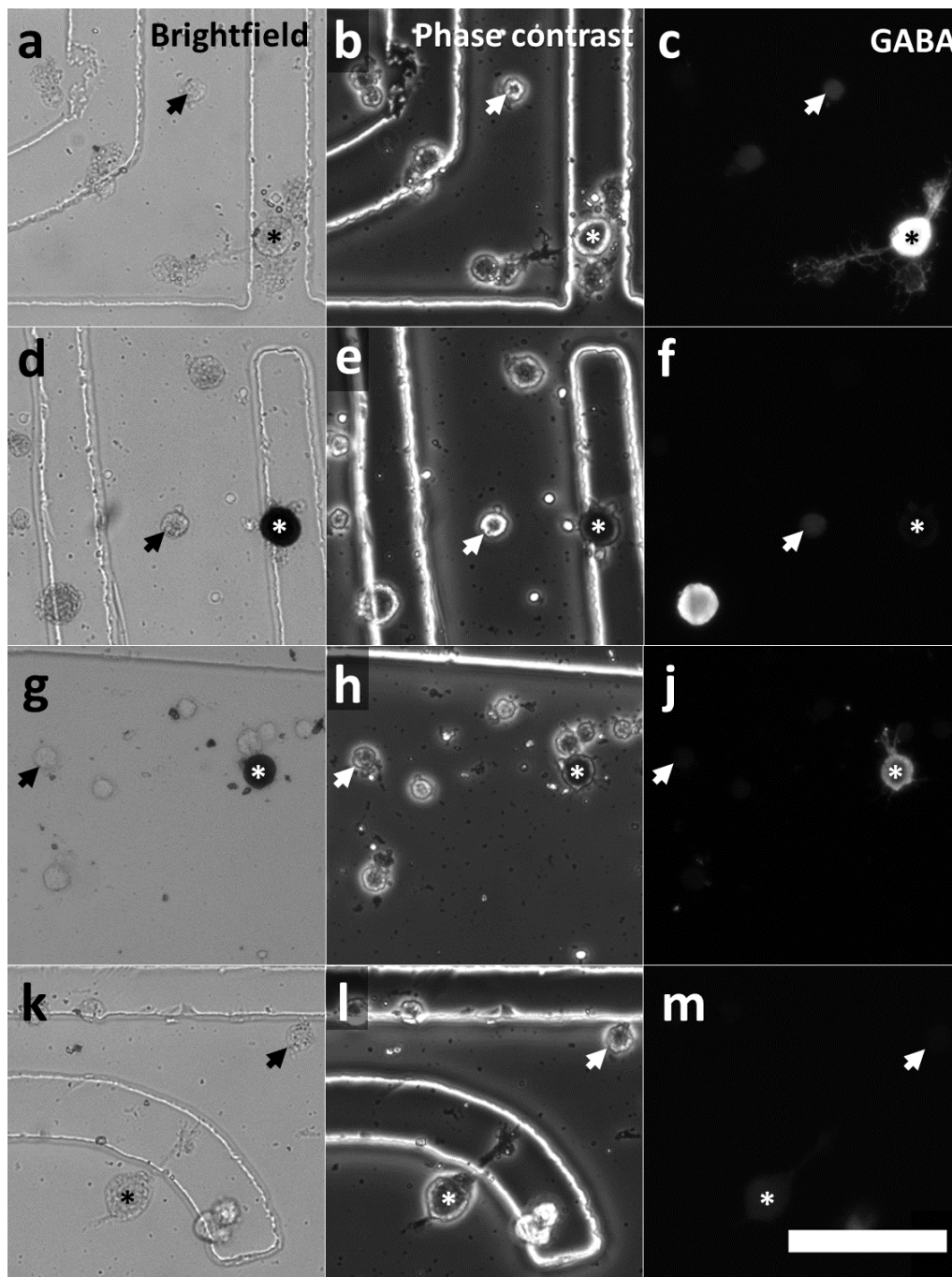
Figure 2: Cellular phenotypes of cultured antennal lobe neurons. Adherent neurons of different soma diameter were grown in petri dishes that contained a numbered location grid for proper cell identification after calcium imaging. Small neurons with soma diameter of about 15 µm are considered as PN (arrows), whereas large neurons of soma diameters above 19.61 µm are regarded to be LN (asterisk). NADPHd activity and GABA-IR was detected in large neurons. LN were classified into four types: exclusively GABAergic (**a-c**); NADPHd positive (**d-f**); GABA-IR and NADPHd positive (**g-j**); LN with no determined (ND) transmitter (**k-m**). Note that LN are generally larger in diameter, but not homogenous in size. Interneurons showing GABA-IR are common, but not morphologically distinct from other non GABA local neurons. LN expressing nitric oxide synthase were detected using NADPHd staining as marker(**d, g**). NADPHd staining tends to quench the fluorescence of GABA-IR local neurons (**j**). Large unlabeled LN showing neither NADPHd activity nor GABA-IR (**k-m** asterisk). Scalebar = 100 µm.
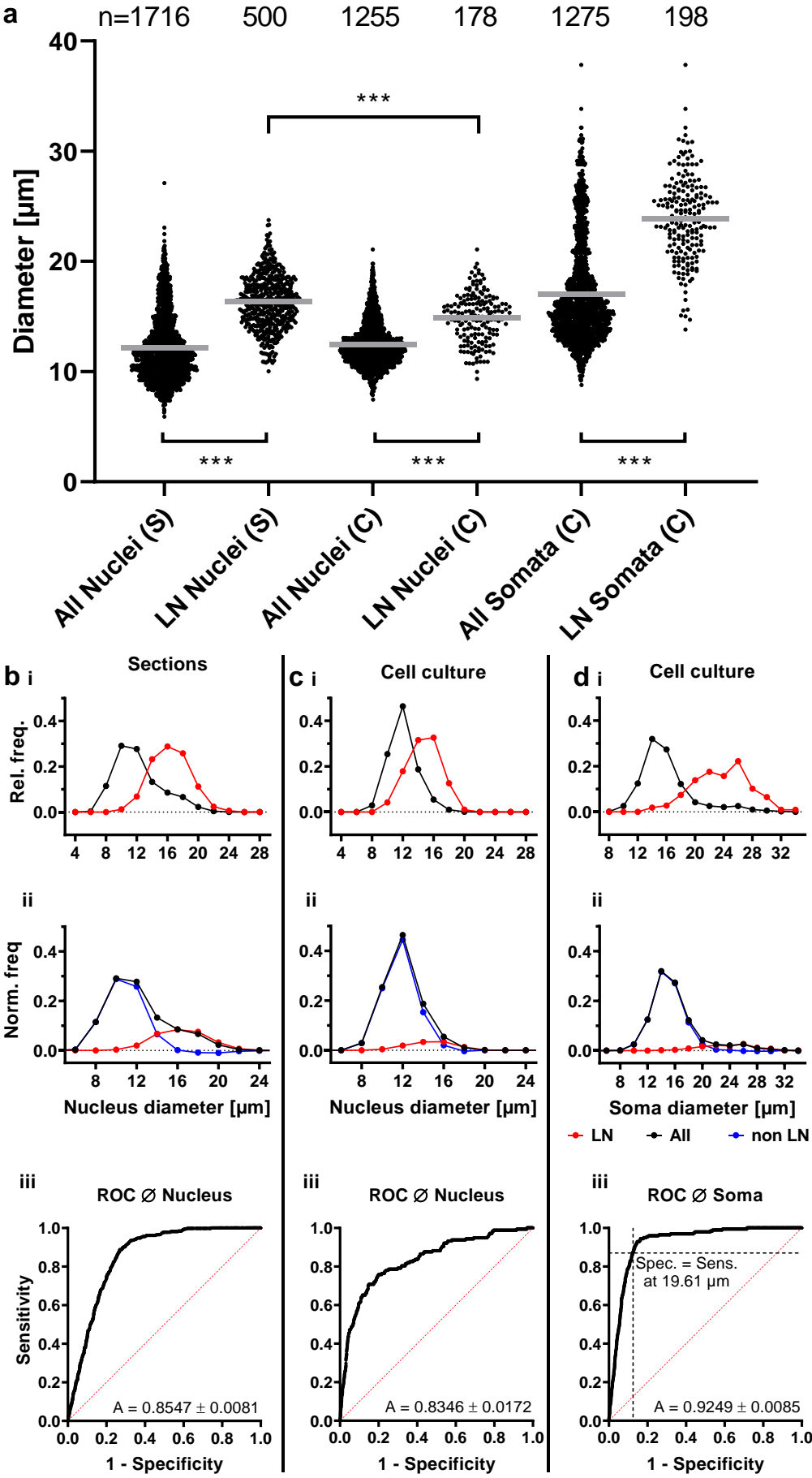
22

1

1   **Figure 3: Discrimination of local and projection neurons based on nucleus and soma diameter.**
2   Individual size measurements of nuclei and somata in sections (S) and culture (C) including respective
3   mean (gray line) are shown in **a**. Nuclear or soma diameters of labeled LN were significantly larger than
4   respective pooled diameters of all neurons in sections and culture ($p < 0.0001$; Kruskal-Wallis test).
5   Nuclear diameters of labeled LN were significantly smaller in culture than in sections ($p = 0.0001$,
6   Kruskal-Wallis test), due to losses during dissociation and culturing. Relative frequencies of pooled
7   nuclear diameters of all cells (including LN) in black, and labeled LN in red, as determined in sections
8   (**b i**) and culture **(c i)**. **d i** shows relative frequencies of soma diameters of corresponding cultured
9   neurons shown in **c**. In **b-d ii** frequencies were normalized to cell counts of all cells. Subtraction of
10 normalized LN frequencies (red) from the pooled cell frequencies (black) resulted in a distribution of
11 neurons without LN (non LN; blue). Non LN frequency at the mean nuclear/soma diameter was close
12 to zero. This allowed estimation of the number of LN in sections (24 %) and culture (10.2 %). For binary
13 LN/PN classification, ROC curves of the classifiers nuclear and soma diameter were plotted (**b-d iii**).
14 The area under the ROC curve (A in **b-d iii**) reflects classifier suitability. For classification of cultured
15 neurons, a threshold soma diameter for discrimination of LN from PN was derived at a value 19.61 µm,
16 accounting for equal classifier specificity and sensitivity (i.e. equal false positive and false negative rate;
17 **d iii**).

24
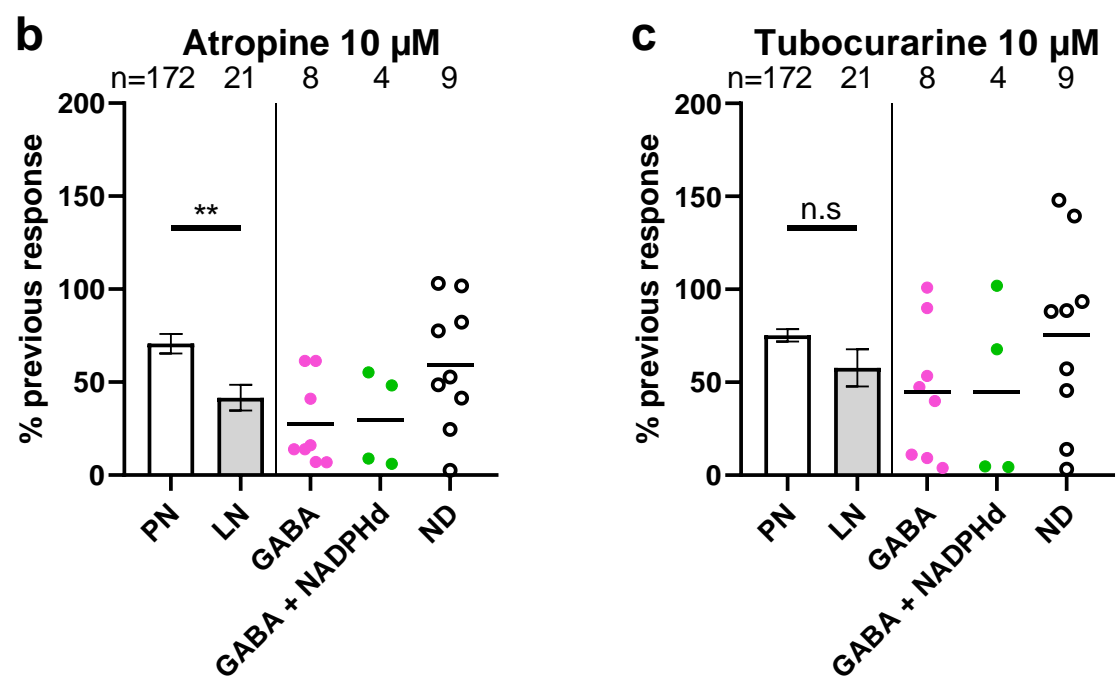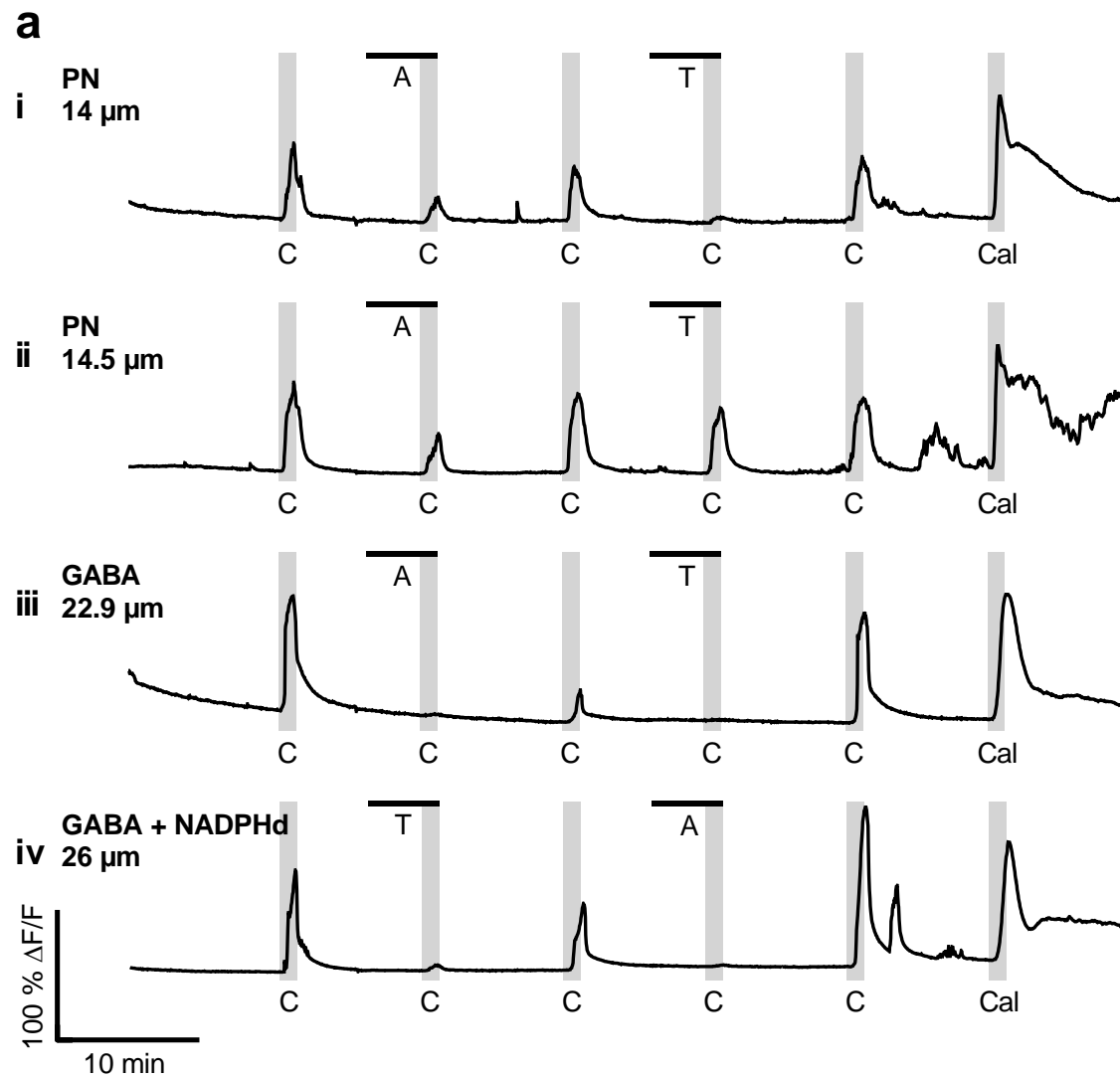
Figure 4: Reduction of carbachol-induced Ca^{2+} transients by co-incubation with cholinergic antagonists. At 10 µM, carbachol elicited Ca^{2+} transients, which were reduced when neurons were also exposed to 10 µM atropine or tubocurarine. Examples for Ca^{2+} signals of PN and LN are shown in **a i-iv**, illustrating the magnitude of reduced transients in individual neurons. The PN in **a i** showed stronger inhibition by the nicotinic antagonist tubocurarine than by the muscarinic antagonist atropine, whereas the PN in **a ii** showed a converse response. Labeled LN (GABA and GABA+NADPHd) showed generally stonger inhibition by antagonists up to a complete response abolishment (**a iii** & **iv**). This reduction of Ca^{2+} responses is summarized in **b** and **c** by normalization of amplitudes in the presence of antagonists to amplitudes prior to antagonist application. Bars show means ± s.e.m. of pooled PN and LN. Colored datapoints represent subtypes of individual LN. Atropine reduced responses of PN to 70.68 % (± 5.29 s.e.m. n=172), and to 41.64 % (± 6.95 s.e.m. n=21) for LN shown in **b**. These reductions were significantly different (p = 0.0048, Mann-Whitney test). As shown in **c,** tubocurarine reduced responses of PN to 75.25 % (± 3.39 s.e.m. n=172), and to 57.74 % (± 9.94 s.e.m. n=21) for LN, which were not significantly different (p = 0.0960, Mann-Whitney test).

1

2

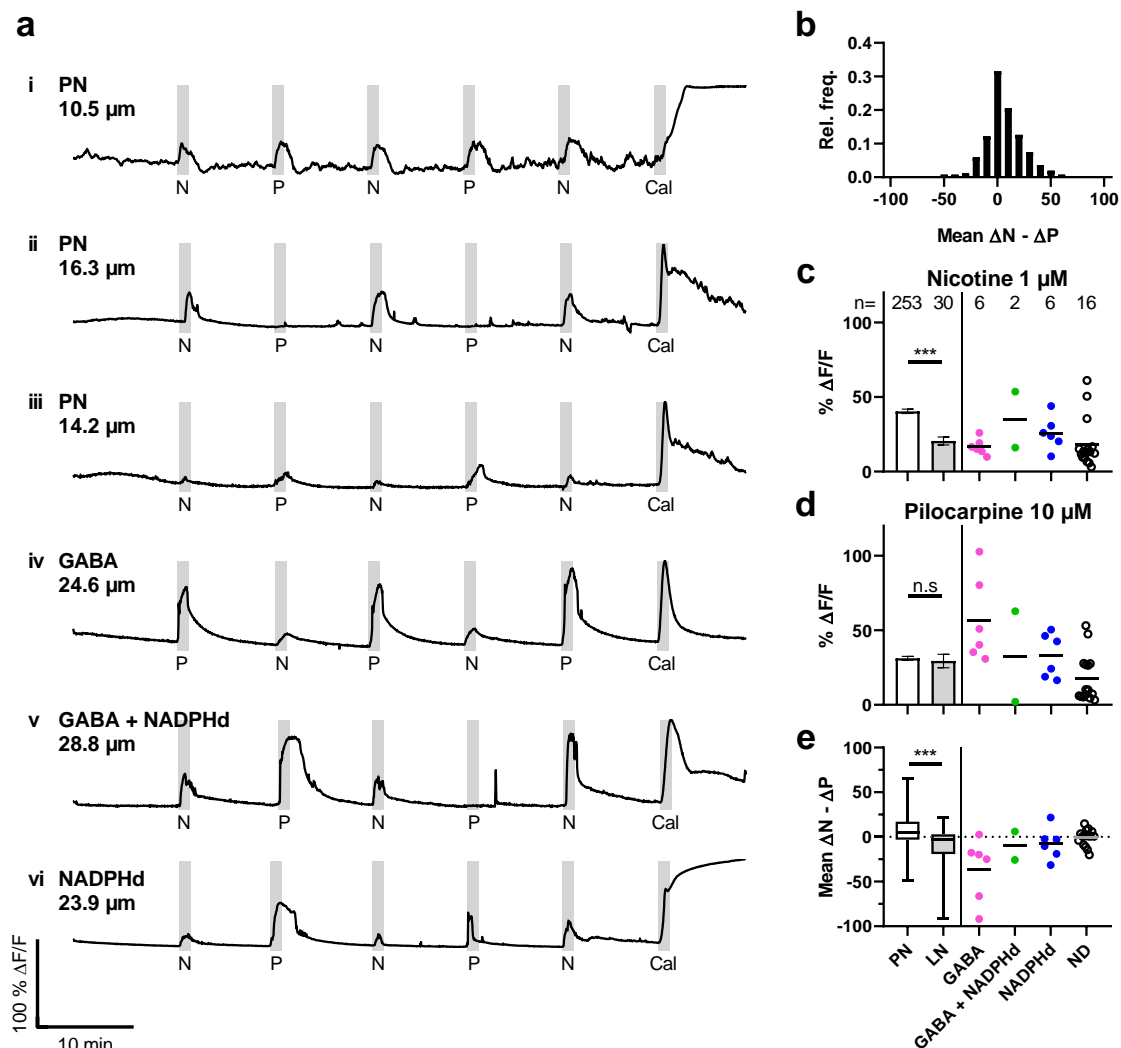**Figure 5: Nicotine and pilocarpine induced-Ca^{2+} transients of cultured antennal lobe neurons.**
Representative Ca^{2+} signals of PN (**i-iii**) and LN (**iv-vi**) are shown in **a**. PNs show three response types
(equal **i**; stronger nicotinic **ii**; stronger muscarinic **iii**). A histogram (**b**) illustrates the distribution of
these types as difference in response amplitude, with 31.6 % of PN showing equivalent responses.
Mean amplitudes (± s.e.m.; normalized to calcimycin) of pooled PN and LN during stimulation with
1 µM nicotine (PN: 40.41 % ΔF/F ± 1.45 s.e.m.; LN: 20.51 % ΔF/F ± 2.69 s.e.m.) or 10 µM pilocarpine
(PN: 31.24 % ΔF/F ± 1.27 s.e.m.; LN: 29.38 % ΔF/F ± 4.51 s.e.m.) are depicted in **c** and **d**. Colored data
points represent subtypes of individual LN. During nicotinic stimulation, Ca^{2+} transients of PN were
significantly larger than those of LN (p < 0.0001; Mann-Whitney test). When stimulated with
pilocarpine no significant differences between PNs and LN were observed (p = 0.3825; Mann-Whitney
test). Amplitude difference between nicotine and pilocarpine induced responses (ΔN - ΔP; **e**) is used to
quantify the relationship between nicotinic and muscarinic responses in individual neurons (PN: 6.84
% ΔF/F ± 1.13 s.e.m.; LN: -9.77 % ΔF/F ± 4.17 s.e.m.). LN show a significant difference to PNs (p <
0.0001; Mann-Whitney test).

1

2

3

28
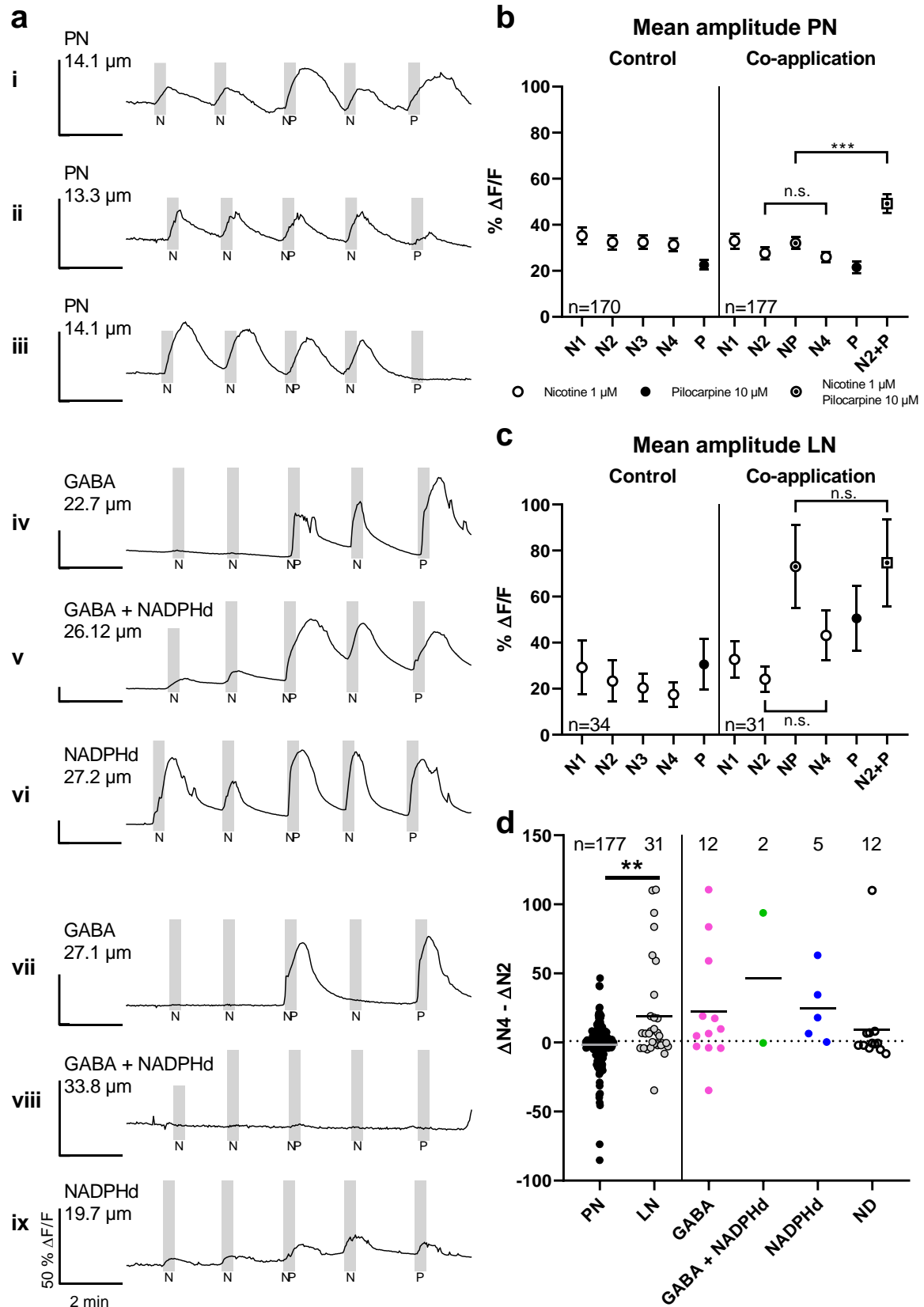
Figure 6: Ca^{2+} response alterations by interaction of muscarinic and nicotinic stimulation. To test for lasting response alterations, a series of two 15s pulses of 1 μM nicotine, one pulse of a 1 μM nicotine and 10 μM pilocarpine mix (no pilocarpine in controls), one nicotine test pulse and one pilocarpine pulse were given in consecutive order. **a** shows examples of Ca^{2+} signals in the co-application protocol. Note that scale varies for better visibility, but all represent 50 % ΔF/F. **a** shows various traces of PN (**i** - **iii**) and different LN types (**iv-ix**). Nicotinic responses were enhanced after co-application in several LN of all types (**a iv** - **vi**), but not in PN. This response enhancement was not found in all of the sampled LN (**a vii** - **ix**). **b** and **c** depict mean Ca^{2+} responses (± s.e.m.) of PN and LN normalized to calcimycin response. Responses to nicotine (empty circle), pilocarpine (filled circle), or nicotine/pilocarpine mix (circled dot) are shown in order of application. The predicted N2+P value (squared dot) was calculated as the sum of individual nicotine and pilocarpine responses during co-application. These predicted responses were significantly different to the respective co-application response in PNs ($p < 0.0001$; Friedman test), but not in LN ($p = 0.1802$; Friedman test). In PNs as well as LN (**b** & **c**), nicotinic amplitudes before and after co-application were not significantly different to each other ($p > 0.9999$ respectively; Friedman test). To account for variability in baseline responsiveness, amplitude differences of nicotinic stimulations after (N4) and prior to co-application (N2) of individual PN (black), LN (gray) and their respective subtypes were calculated (**d** line represents mean). Amplitude differences of LN were significantly different to those of PNs ($p = 0.0073$; Mann-Whitney test), demonstrating an enhancement of nicotinic responses after co-application of the muscarinic and nicotinic agonists.